Article

Structural, Dielectric and Thermal Properties of Pb Free Molybdate Based Ultra-Low Temperature Glass

Jobin Varghese, Tuomo Siponkoski, Merja Teirikangas, Mailadil Thomas Sebastian, Antti Uusimaki, and Heli Jantunen

ACS Sustainable Chem. Eng., **Just Accepted Manuscript** • DOI: 10.1021/acssuschemeng.6b00721 • Publication Date (Web): 07 Jun 2016

Structural, Dielectric and Thermal Properties of Pb Free Molybdate Based Ultra-Low Temperature Glass

Jobin Varghese*, Tuomo Siponkoski, Merja Teirikangas, Mailadil Thomas Sebastian, Antti Uusimäki and Heli Jantunen

Microelectronics Research Unit, Faculty of Information Technology and Electrical Engineering, University of Oulu, Finland, P.O. Box 4500, FI-90014.

*jobin.var@gmail.com

KEYWORDS (ULTCC; Glass; X-ray diffraction; XPS analysis; Raman spectroscopy; Coefficient of thermal expansion; Dielectric properties).

ABSTRACT: A new glass with ultra-low glass transition temperature based on $10Li_2O$-$10Na_2O$-$20K_2O$-$60MoO_3$ (LNKM) has been developed by conventional glass melting and quenching process. The glass has ultra-low glass transition and melting temperatures being 198 ^oC and 350 ^oC respectively. The glass exhibits a coefficient of thermal expansion of 17 ppm/^oC in the temperature range of 25-300 ^oC. X-ray diffraction and Raman spectroscopic studies indicate that the glass is partially crystallized. The chemical and elemental composition of the glass is confirmed by X-ray photoelectron spectroscopy. The glass pellet heat treated at 300 ^oC has a relative permittivity of 5.07 and dielectric loss tangent of 0.006 at 1 MHz. At 9.97 GHz, it shows a relative permittivity of 4.85 and dielectric loss tangent of 0.0009. The temperature dependence of the relative permittivity at 1 MHz and 9.97 GHz of the glass is 307 ppm/^oC (temperature range 20-100 ^oC) and 291 ppm/^oC (temperature range 25-85 ^oC) respectively.

INTRODUCTION

In the past two decades, glass materials have been established as an ideal packaging materials for microelectronic devices.[1, 2] The main applications of low melting point glasses are in batteries[3], optoelectronic devices[1, 2], hermetic sealing[1, 2], encapsulation of semiconductor devices [1, 2], photovoltaics [1, 2, 4], and thick film electronics, *etc.*,.[5, 6] Among these glasses, Pb rich glasses with low

melting point are extensively used for various electronic and other packaging applications.[1, 2] However, Pb-based materials are toxic to human health and the environment.[7] Recently, several new glass ceramic compositions with good dielectric properties have been developed for microwave applications.[8] Many of the Low and Ultra-Low Temperature Co-fired Ceramics (LTCC, ULTCC) utilizing low melting point glasses are able to offer significant benefits over other traditional packaging techniques.[9-12] As a multilayer technology, conductive lines, vias, sensors, antennas or other components have been embedded to the LTCC based packages with good hermetical and thermal management.[13-18] Lead free inorganic functional materials are also getting more attention at present scenario. [19] Avoiding toxic materials like Pb is also essential when ULTCC and LTCC compositions are developed.

Over the last two decades, several approaches such as chemical synthesis[20, 21], use of starting powders with smaller particle size[22] and liquid phase sintering by adding low melting additives[21, 22] have been adopted for reducing the sintering temperature of low loss ceramic materials. There are several recent reports on ultra-low temperature sinterable ceramic materials with and without glass addition.[23-26] Glasses with good dielectric properties for LTCC materials processing are also reported in the literature and are commercially available.[27] Most of the reported low-temperature glasses are PbO-B_2O_3 based usually with additives such as SiO_2, ZnO and Al_2O_3 having glass transition temperature, relative permittivity and Qf in the range of 390- 500 ^oC, 10-20 and 500-1000 GHz respectively.[1, 26, 27] The ULTCC materials can be classified into category I (sintering temperature $\leq$ 400 ^oC) and category II (sintering temperature > 400-700 ^oC) materials. Classification of these ultra-low temperature ceramics is based on electrode metal compatibility as well as low-temperature fabrication process with environmentally friendly materials.[26] Recently, several materials such as $LiMoO_4$, $LiMoO_4$-TiO_2, $LiMoO_4$-$BaTiO_3$, $BaTiO_3$-BBSZ, and $NaAgMoO_4$ are reported for ULTCC Category I applications.[28-31]

In addition to the low sintering temperature, ULTCC materials should also have good dielectric, thermal and mechanical properties being important factors for device level integration. Most of the reported category II materials include lithium, sodium, potassium, bismuth, silver, tellurium, lead, based molybdates with sintering temperatures in the range of 400-700 ^{o}C.[23, 26, 32-43] These materials have relative permittivity in the range of 5-45 and quality factor (Qf) of 1,000-70,000 GHz.[32-43] More recently, MoO_3 with an orthorhombic structure consisting of corner sharing and edge-sharing MoO_6 octahedra has showed potential applications. [44, 45] In the modern scientific world, molybdates based materials and glasses are getting more attention in technology as well as in materials research. [46-50] The primary objective of present study is to develop environment friendly ULTCC category I composition based on $10Li_2O$-$10Na_2O$-$20K_2O$-$60MoO_3$ (LNKM). The preparation, structural, thermal and dielectric properties of bulk LNKM glass heat treated at 300 ^{o}C are presented.

EXPERIMENTAL SECTION

Materials. The lithium sodium potassium molybdate glass consists of 10 mol. % Li_2O - 10 mol. % Na_2O – 20 mol. % K_2O - 60 mol. % MoO_3 (LNKM), was prepared by conventional melting and quenching process. High purity chemical raw materials, Li_2CO_3 (> 98 % Sigma Aldrich), Na_2CO_3 (> 99 %, Sigma-Aldrich), K_2CO_3 (99 %, Merck) and MoO_3 (Alfa Aesar, 99.5 %), were mixed with agate mortar and pestle. The mixed materials were melted at two different temperatures at 400 and 500 ^{o}C for 1 h in a Pt crucible, and quenched at ice-cold ethanol bath. The quenched glass was milled using yttria-stabilized zirconia (YSZ) balls in absolute ethanol medium for 12 h and dried in an oven at 80 ^{o}C. The dried powder was then pressed into cylindrical discs of 14 mm in diameter and ~1.8 mm in thickness for LCR and impedance analyzer measurements, and 25 mm in diameter and ~ 0.7 mm in thickness for SPDR (Split Post Dielectric Resonator) measurements. The samples were heat treated at 300 ^{o}C/2h with a heating rate of 5 ^{o}C/min and cooling rate of 3 ^{o}C/min.

Methods. The crystallinity of the powdered glasses was analyzed with X-ray diffraction technique (D8, Bruker, Billerica, MA) using CuKα radiation. XPS measurements were performed with a Thermo Fisher Scientific, ESCALAB 250 Xi using the MgKα X-ray source. The spectrometer was calibrated using the reference energies of Au $4f_{5/2}$ (83.9±0.1 eV) and Cu $2p_{3/2}$ (932.7±0.1 eV). A take-off angle of 90^{o} was used (angle between the surface and the analyzer). A binding energy of 285.0 eV assigned to the C 1s peak corresponding to the surface contamination and this was used as an internal reference for correction of charging effects. The glass transition temperature and crystallization of the glass were analyzed using TG/DSC (NETZSCH, STA 499 F3 Jupiter, Germany) at a heating rate of 2 ^{o}C/min. Glass deformation and coefficient of thermal expansion (CTE) were investigated using dilatometer (NETZSCH, DIL 402 PC/4, Germany) with a heating rate of 5 ^{o}C/min in the temperature range of 25-300 ^{o}C. The optical Raman spectra were measured using spectrometer (LabRam HR800, Horiba Jobin-Yvon, Villeneuve-d'Arcy, France) with signals excited by a 488 nm Ar^{+} laser. The dielectric properties from 20 Hz to 1 MHz were measured using Precision LCR meter (Agilent 4284A, Precision LCR Meter, USA) with accuracy of measurement of 0.1 %. The temperature dependence of relative permittivity in the range of 20-100 ^{o}C was also measured using Precision LCR meter. The dielectric properties from 5 MHz to 1 GHz were measured using RF impedance/Materials Analyzer (E4991A, Agilent, Santa Clara, CA) with Agilent 16453A dielectric material test fixture with an accuracy of 1 %. The relative permittivity, dielectric loss and temperature dependence of the permittivity (temperature range 25-85 ^{o}C) were measured by SPDR method with nominal resonance frequency of 9.97 GHz using a Vector Network Analyzer (10 MHz-20 GHz, ROHDE& SCHWARZ, ZVB20, Germany). The total uncertainty of the relative permittivity in SPDR measurement method does not exceed 0.5 %, and it is possible to resolve dielectric loss tangents to approximately $5x10^{-5}$.[51]

RESULTS AND DISCUSSION

XRD analysis. Figure 1 (a), (b) and (c) illustrates the X-ray diffraction pattern of glass quenched from 400 ^{o}C, 500 ^{o}C and heat treated glass powder (quenched from 500 ^{o}C) at 300 ^{o}C respectively. The partially crystalline phase observed from the XRD pattern of the glass quenched from 400 ^{o}C belongs to the Li, Na, K molybdates crystallites.

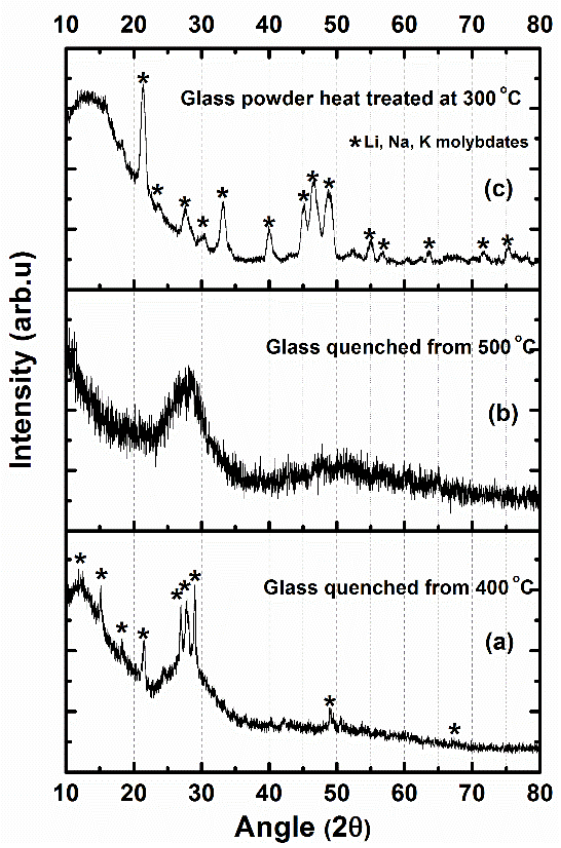

Figure 1 X-ray diffraction pattern of LNKM glass (a) quenched from 400 ^{o}C, (b) 500 ^{o}C and (c) quenched from 500 ^{o}C and powder heat treated at 300 ^{o}C.

However, the glass quenched from 500 ^{o}C (See the photographic and optical image of LNKM glass quenched from 500 ^{o}C is shown in the supporting information, Figure S1) revealed amorphous nature as presented in Figure 1 (b). The heat treated powder showed several partially crystalline phases (Figure 1 (c)) such as Li_2MoO_4 (ICDD file card No: 12-0763), Na_2MoO_4 (ICDD file card No: 00-012-0773), $K_2Mo_3O_{10}$ (ICDD file card No: 37-1467), $K_2Mo_2O_7$ (ICDD file card No: 27-0416) and $K_2Mo_4O_{13}$ (ICDD file card No: 36-0347). It is also reported that Na_2MoO_4 retains its spinel structure (α

-Na_2MoO_4, ICDD file card No: 00-012-0773) until 400-460 ^oC, and it becomes orthorhombic (β form) and finally hexagonal (γ form) above 650 ^oC before melting (~ 690 ^oC).[52]

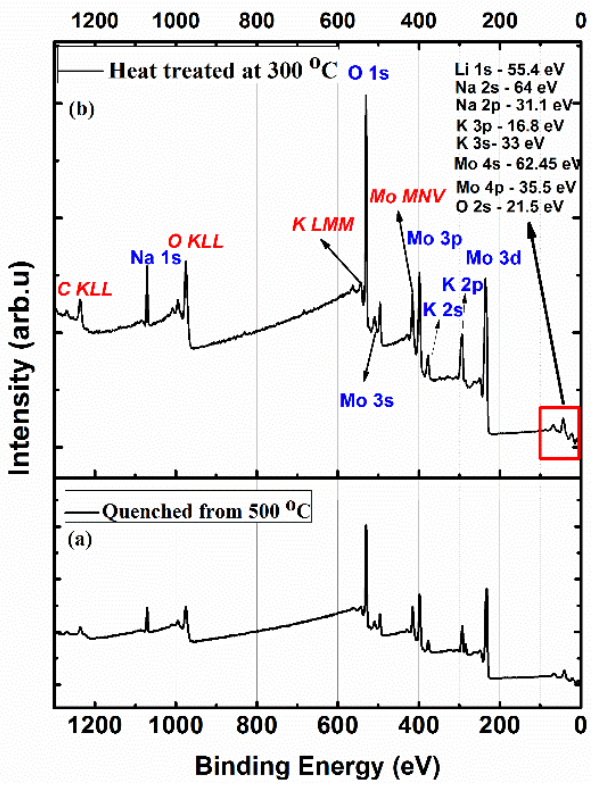

Figure 2 XPS survey spectrum of LNKM glass (a) quenched from 500 ^oC and (b) bulk sample heat treated at 300 ^oC.

XPS analysis. The chemical composition and oxidation state of the MoO_3 rich LNKM glass were analyzed by using XPS technique. A qualitative analysis of the chemical state of the LNKM glass quenched from 500 ^oC and bulk glass sample heat treated at 300 ^oC, within the surface layer of about 50 Å, is extracted from the spectrum. The survey spectrum of LNKM glass sample quenched from 500 ^oC and bulk glass sample heat treated at 300 ^oC are shown in Figure 2 (a) and (b) respectively. Besides the expected Li 1s, Na 1s, K $2p_{1/2}$, $2p_{3/2}$, Mo $3d_{5/2}$, $3d_{3/2}$, O 1s peaks, a C 1s peak were also observed. The C 1s peak appears due to the adsorption of hydrocarbon impurities. This peak does not affect the interpretation of the present results and in fact, it was used for binding energy calibration by setting its binding energy at 284.8 eV in order to correct the sample charging.[53] Figure S2 (Supporting

Information) shows the high resolution spectrum of C 1s peak originating from the hydrocarbon impurities present at the surface of LNKM glass. It is evident that the lowest peaks appearing below the binding energy 100 eV are attributed to the peaks corresponding to the Li 1s, Na 2s & 2p, K 3s & 3p, Mo 4s and O 2s. Rastogi *et. al.,* and Nyholm *et. al.,* reported the low binding energy orbitals of Mo 4p, $4p_{3/2}$, and 4s at 35.3, 35.5 and 63.2 eV, respectively.[54, 55]

In the survey spectrum, Auger lines of Mo (415 eV) are also evidently belonging to the Auger line of AP-$3d_{5/2}$, M45N23V and are reported by Powell *et. al.,* in 2012.[56] The peak corresponding to Mo $3p_{1/2}$, $3p_{3/2}$ and 3s is also visible in the survey spectrum of the LNKM glass. All the above peaks of Mo are indexed based on previous reports as well as NIST XPS database.[57-59]

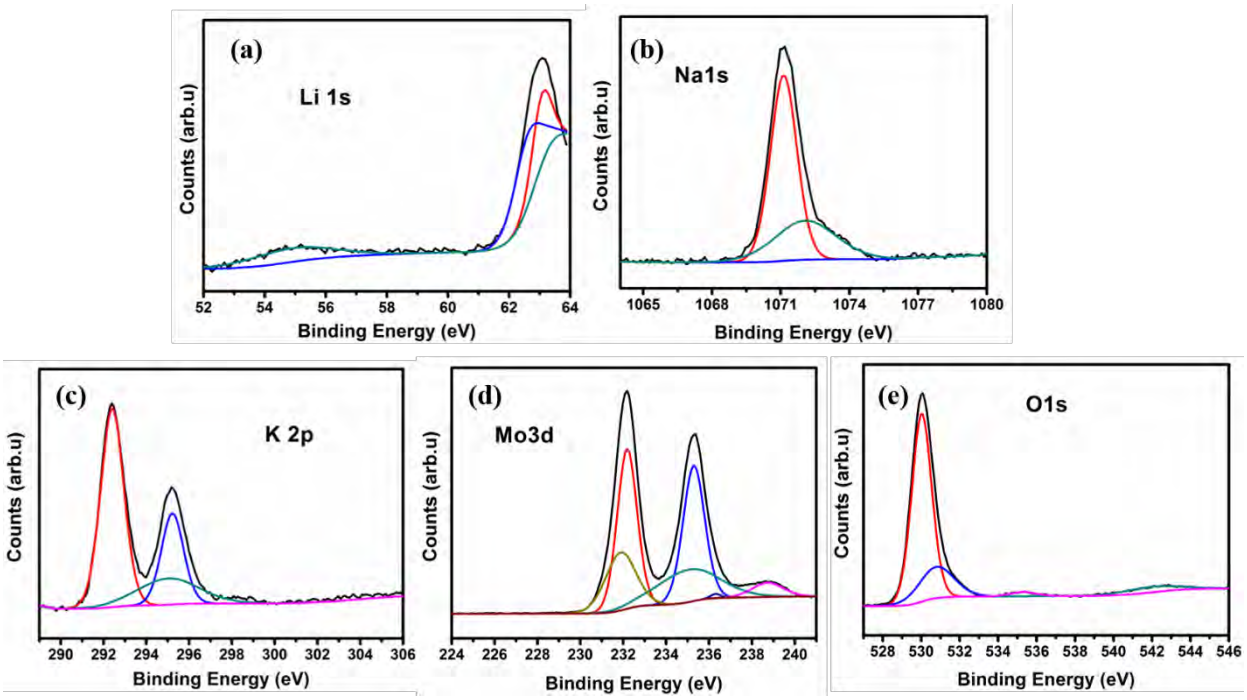

Figure 3 High resolution XPS spectrum of (a) Li 1s, (b) Na 1s, (c) K 2p, (d) Mo 3d and (e) O 1s from LNKM bulk glass sample heat treated at 300 ^{o}C.

The high-resolution Li 1s spectrum consisting of two weak peaks are evident from Figure 3 (a). In XPS, Li sensitivity is limited to 10 mol. % of Li_2O in the LNKM glass and it is hard to study the high-resolution Li spectrum. However, a high-resolution spectrum of a weak Li 1s peak is also detected at

54.33 eV with atomic wt. % of 1.33 and the peak fitted at 62.45 eV may be due to the peaks of Mo 4s with atomic wt. % 3.86. It is reported that Mo has 4s orbital peak at 62.45 eV which is close to the observed spectrum of LNKM glass.[54] The XPS spectral resolution is limited to lower binding energy region below 100 eV. High-resolution Na 1s spectrum and the fit parameters to the Na 1s spectrum of LNKM glass are illustrated in Figure 3 (b). Generally, glass materials may exhibit increased amount of sodium at the surface due to diffusion processes. However, the present LNKM glass contains only 10 mol. % Na_2O and the peak fitted for Na 1s spectrum has a dominant peak at 1071.15 eV at atomic wt. % of 4.56 observed and shoulder peak matched at 1072.96 eV with atomic wt. % of 0.9 which may belong to the bridging oxygen atom present in the LNKM glass.[60]

Figure 3 (c) represents the high-resolution spectrum of K 2p in the LNKM glass. The peaks correspond to K 2s and K 2p also noted in the survey spectrum of LNKM glass (Figure 2). The K 2p spectrum exhibits a principal peak fitted at low binding energy 292.43 eV belonging to the peak of K $2p_{3/2}$ with atomic wt. % of 7.9 and another peak matched at little higher binding energy 295.21 eV which is attributed for K $2p_{1/2}$ with atomic wt. % of 5.25. This is due to the spin-orbit splitting doublet composed of two peaks of K 2p and is reported by Nefedor *et. al.,*.[61, 62] High-resolution spectrum of Mo determines the elemental composition and oxidation state of Mo in the LNKM glass. Figure 3 (d) shows the high-resolution spectrum of Mo 3d orbitals such as Mo $3d_{3/2}$ and $3d_{5/2}$ at 232.13 and 235.28 eV with atomic wt. % of 24.61 and 21.42, respectively. This Mo 3d line indicates only Mo^{6+} oxidation state for LNKM glass. Similar observation was also reported.[63] High-resolution spectrum of O 1s and its curve fitting for LNKM glass are shown in Figure 3 (e). These O 1s photoelectron peaks provide information on the oxide ion in the molybdates glass with different chemical bonding. A well-resolved peak around 530.03 eV fitted with atomic wt. % of 21.84 is associated with the Mo-O-Mo vibrations (bridging oxygen group), accompanied by shoulder peak fitted at 531.07 eV with atomic wt. % 4.41

associated with Mo-O-Li, Mo-O-Na and Mo-O-K glass modifiers present with the content of 10 mol. % Li_2O- 10 mol. % Na_2O- 20 mol. % K_2O- 60 mol. % MoO_3. All the peaks associated with O 1s show good agreement with reported values of alkali-molybdates.[61,64]

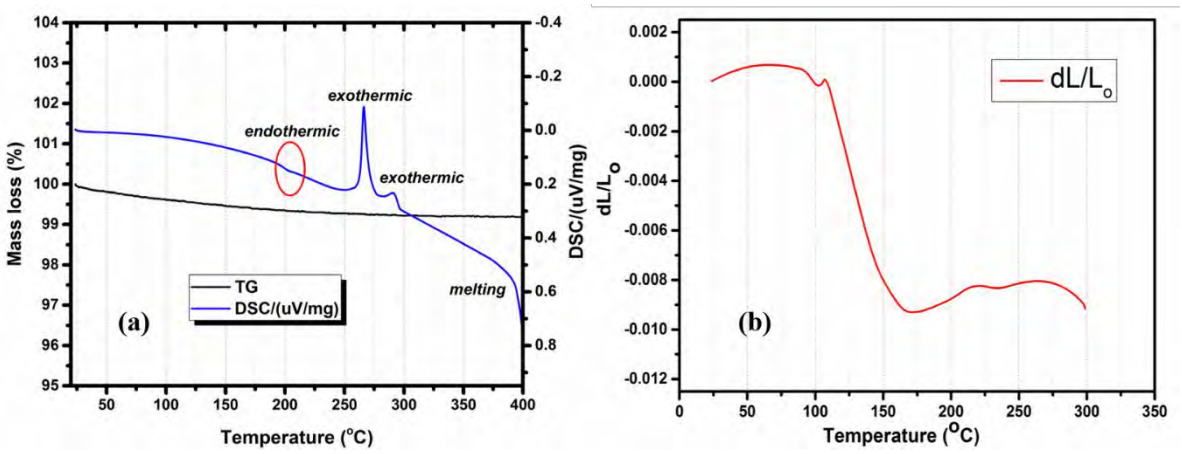

Figure 4 (a) TG and DSC curve of quenched glass from 500 °C and (b) Shrinkage measurement at temperature range of 25-300 °C.

Thermal analysis and coefficient of thermal expansion. The TG/DSC analysis of LNKM glass at a heating rate of 2 °C/min (glass quenched from 500 °C) is depicted in Figure 4 (a). The DSC curve of LNKM glass shows first endothermic peaks near to 195-200 °C which corresponds to the glass transition temperature. The observed Tg of the glass is at 198 °C. The two exothermic peaks present in the temperature range of 250-300 °C correspond to the crystallization of Li, Na, K molybdates. The high field strength of Mo^{6+} cation and crystallization of alkali molybdates may occur during the melt cooling or heat treatment of glass. It has been reported that Mo^{6+} cation exerts a strong ordering effect on the surrounding anions and combine with other elements such as alkali and alkali-earth cation to form crystalline molybdates.[53-56] The area under the exothermic peaks (DSC curve) is proportional to the quantity of the crystallization. The massive crystallization during heat treatment might be due to the seeding effect of MoO_3 present in the glass composition. The melting of LNKM glass occurs at 350 °C.

Figure 4 (b) shows the shrinkage measurement of LNKM glass pellet over a temperature range of 20 - 300 °C. The shrinkage analysis shows similar behavior as that of DSC measurement in Figure 4 (a). The shrinkage measurement further confirms that the glass softening temperature of the LNKM glass is about at 100 °C. The LNKM glass shows bulk Archimedes density of 3.05 g/cm^3 using absolute ethanol medium. Among the crystalline molybdates, alkali molybdates are water soluble ceramics and are suitable for ultra-low temperature materials and its processing.[28, 29, 31] Figure 5 shows the variation of linear change in length as a function of temperature of LNKM glass heat treated at 300 °C. The LNKM glass shows an average CTE (coefficient of thermal expansion) of about 17 ppm/°C in the temperature range of 25-300 °C.

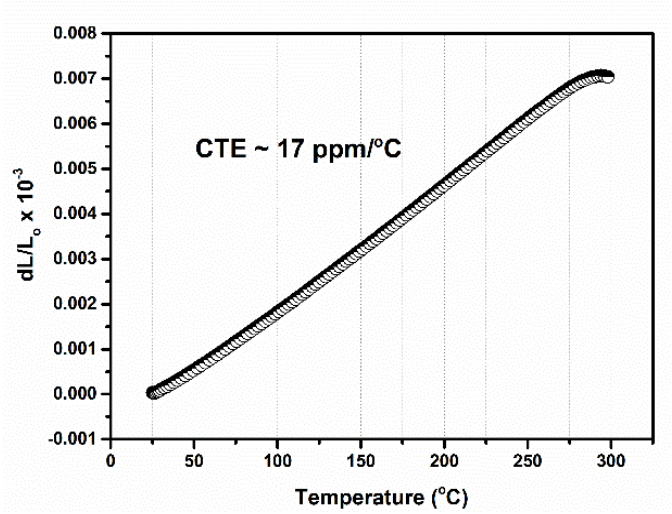

Figure 5 Temperature variation of change in linear dimension (25-300 °C) of bulk LNKM glass pellet heat treated at 300 °C.

Raman spectrum analysis. Figure 6 (a), (b) and (c) show Raman spectra of LNKM glass heat treated at 300 °C, quenched from 500 °C, and pure MoO_3 pellet heat treated at 500 °C respectively. According to the group theory analysis of MoO_3, 45 optical modes are expected at k = 0 for the D_{2h}^{16} (Pbnm) space group and 24 of them are Raman active ($8Ag + 8B_{1g} + 4B_{2g} + 4B_{3g}$).[65] The Raman spectra of the alkali-mono molybdates are well documented by Voronko *et. al.,* recently.[66] According to Voronko *et. al.,*

vibrational frequency assignments are ν_2 (E)+ν_4 (F_2) states at a wavelength of 315, 320, 320 cm^{-1}, assigned for Li_2MoO_4, Na_2MoO_4, K_2MoO_4, respectively. The vibrational frequencies and assignments for $\nu_3(F_2)$ are 820 and 815 cm^{-1} and the vibrational state for ν_1 (A_1) at 895, 885, and 870 cm^{-1} relates to Li_2MoO_4, Na_2MoO_4, and K_2MoO_4.[66] In the present studies, Raman spectra are divided into low-frequency region (50-600 cm^{-1}), mid-frequency region (600-900 cm^{-1}) and high-frequency region (900-1250 cm^{-1}) for appropriate discussion.

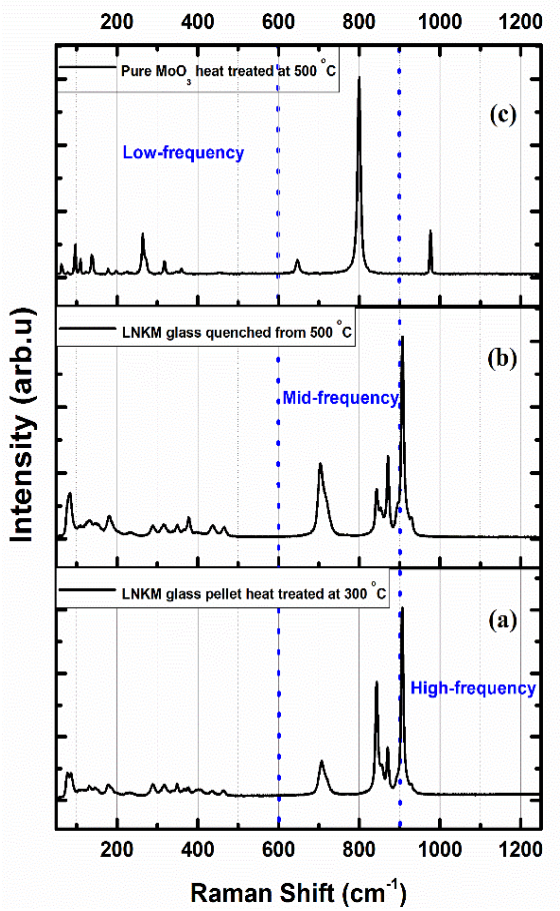

Figure 6 Raman spectra of LNKM glass (a) bulk sample pellet heat treated at 300 °C (b) quenched from 500 °C and
(c) Raman spectra of pure MoO_3 sample heat treated at 500 °C.

Low-frequency region (50-600 cm^{-1}). A few weak peaks are observed in the Raman spectra of LNKM glass as well as pure α-MoO_3 at room temperature in the low-frequency region. The spectra in Figure 6 (a) and (b) show a couple of weak peaks below 600 cm^{-1}, which can be roughly classified as

deformation modes between 450 and 200 cm^{-1} and all other peaks present below 200 cm^{-1} are ascribed as lattice modes.[65] On comparing the Raman spectra of LNKM glass with that of pure MoO_3 (Figure 6 (c)), it is observed that some of the bands at lower wavelength region broaden and some lower frequency lines have disappeared, which is characteristic for lattice modes. It is also evident that weak Raman modes of $v_2(E)+v_4(F_2)$ alkali-mono molybdates are also present in the Raman spectrum of LNKM glass depicted in Figure 6 (a) and (b).[66]

Mid-frequency region (600-900 cm^{-1}). MoO_3 peak at 649 cm^{-1} (Figure 6 (c)) is shifted to the wavelength region of 700-720 cm^{-1} in the spectrum of LNKM glass as seen in Figure 6 (a) and (b). The corresponding peaks of state $v_3(F_2)$ are also present in the Raman spectrum of LNKM glass is shown in Figure 6 (a) and (b). The broadened peak present in the frequency range of 815-830 cm^{-1} corresponds to the peaks of alkali-mono molybdates present in the LNKM glass. It is also reported that the peaks present in the 870-895 cm^{-1} belong to the $v_1(A_1)$ vibrational state of alkali-mono molybdates present in the LNKM glass.[66] There are reports that the sharp line at 848 cm^{-1} is assigned to stretching vibrations of the metal-oxygen bonds in the corner-sharing octahedra in Mo-O-Mo units which are also evident in the LNKM glass.[65]

High-frequency region (900-1250 cm^{-1}). The band around 900-975 cm^{-1} is due to the symmetric stretching vibration of $(MoO_4)^{2-}$ tetrahedral units located in the glassy phase of LNKM glass (Figure 6 (a) and (b)). These bands can be mostly associated with terminal oxygen atoms (Mo=O or Li-O, Na-O, K-O) bond vibrations associated with either 4, 5 or 6 coordinated Mo atom.[67, 68] It is observed that molybdenum oxide rich glass shows that the terminal molybdenum-oxygen bonds are present in the entire glass-forming range. Raman spectra reveal the crystalline nature of the LNKM glass in comparison with XRD and TG/DSC analysis.

Dielectric properties. The Figure 7 (a) shows the relative permittivity and dielectric loss of LNKM partially crystalline glass heat treated at 300 °C as a function of frequency ranging from 20 Hz to 1 MHz. Relative permittivity and dielectric loss show a decreasing trend with an increase in frequency. The relative permittivity decreases from 6.27 to 5.07 with an increase in frequency. The dielectric loss decreases from 0.09 to 0.006 at this frequency range.

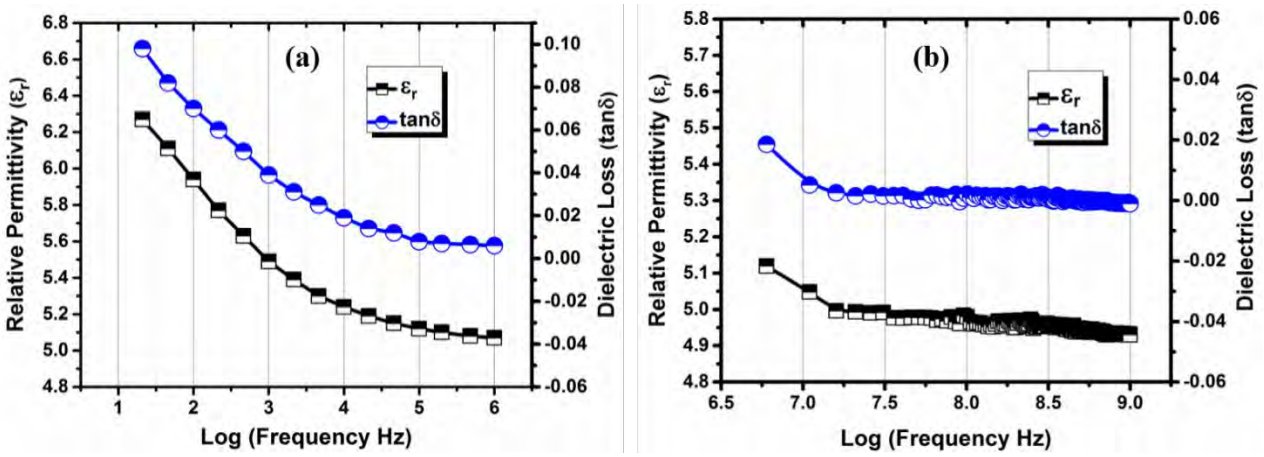

Figure 7 Relative permittivity and dielectric loss of bulk LNKM glass heat treated at 300 °C as a function of log of frequency ranging from (a) 20 Hz to 1 MHz and (b) 5 MHz to 1 GHz.

A similar observations are also visible in the high-frequency region from 5 MHz to 1 GHz measured with an impedance analyzer (Figure 7 (b)), where the relative permittivity decreases from 5.11 to 4.93. The decreases in the relative permittivity, especially at a lower frequency, may be associated with electrode polarization as well as the effect of orientational polarization during the measurement.[69, 70] The dielectric loss tangent decreases from 0.02 to 0.001 at this frequency range of 5 MHz to 1 GHz being moderately low against the earlier reported values for low loss glasses.[27]

The microwave dielectric properties of developed LNKM glass (heat treated at 300 °C) measured using split post dielectric resonator with the nominal resonant frequency of 9.97 GHz shows relative permittivity of 4.85 and dielectric loss tangent of 0.0009. Table 1 depicts the ULTCC category 1 materials and their microwave dielectric properties based on the recent review on ULTCC materials by

Sebastian *et. al.*,.[26] It is noted that only few number of materials and glasses are reported for ULTCC category 1 applications. In comparison with reported ULTCC materials, present LNKM glass shows good microwave dielectric properties.

Table 1 ULTCC category 1 materials and microwave dielectric properties

Materials	ε_r	Qf/tanδ	References
LNKM glass	4.8	0.0009	Present paper
$NaAgMoO_4$	7.9	33,000	26
$PbO\text{-}B_2O_3\text{-}SiO_2$ (50:40:10)	13.8	900	26
$PbO\text{-}B_2O_3\text{-}SiO_2$ (70:20:10)	19.6	500	26
$BBSZ+BaTiO_3$	36	0.007	26

The variation of the relative permittivity of LNKM glass with the temperature at low frequencies (20 Hz, 100 Hz, 1 kHz, 100 kHz and 1 MHz) is shown in Figure 8 (a). A similar behavior of decreasing permittivity (Figure 7) with increasing frequency is observed. It is evident from the Figure 8 (a) that the relative permittivity increases with increase in measuring temperature from 20 to 100 ^oC. When the frequency increases the temperature variation of relative permittivity becomes smaller. The temperature variation of the relative permittivity (τ_ε) of LNKM glass at 1 MHz is about 307 ppm/^oC. The low-frequency dispersion in relative permittivity gradually increases with increase in temperature. This is due to the electrode polarization as well as thermal activation of defect dipole present in the LNKM glass matrix. Similar observations are also reported by Jungang *et. al.,* in 2010.[70]

Figure 8 (b) shows that the temperature variation of relative permittivity (τ_ε) and dielectric loss at 9.97 GHz. The heat treated LNKM glass shows the temperature-dependent of the relative permittivity of 291 ppm/^oC at 9.97 GHz. It shows a similar trend like that of 1 MHz, a slight increase in the relative permittivity with temperature.

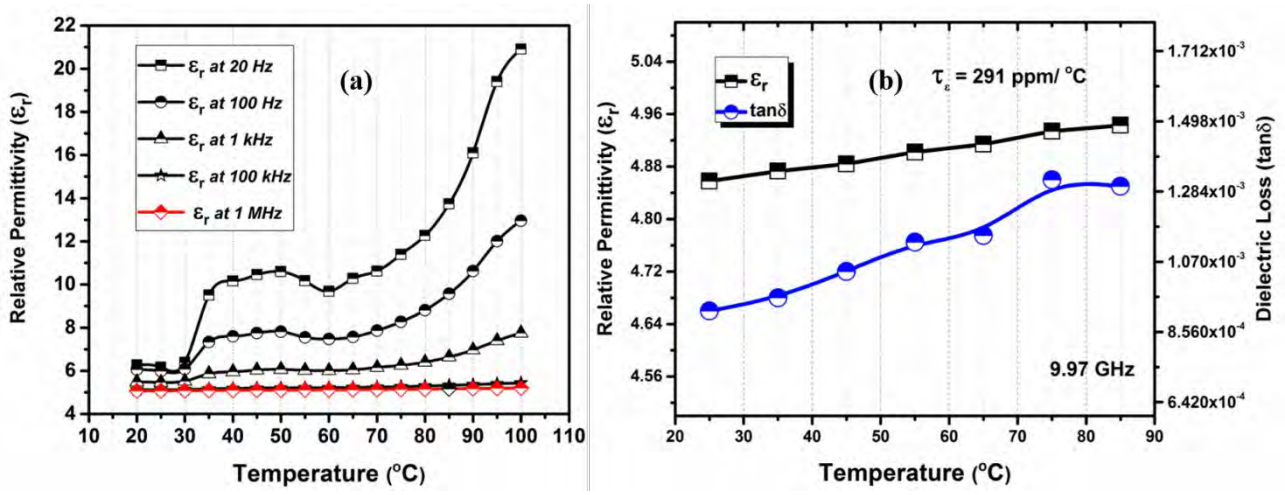

Figure 8 Temperature variation of (a) relative permittivity at various low frequencies and (b) relative permittivity and dielectric loss tangent at 9.97 GHz of bulk LNKM glass heat treated at 300 °C.

The increased dielectric loss during heating at 9.97 GHz is due to the presence of ion–polaron interactions as well as thermal activation dominating in this frequency range. It is assumed that the mobile electrons (polarons) are attracted to oppositely charged Li^+, K^+ and Na^+ ions and create cation–polaron pairs, which move together as neutral- entities.[71,72] Ultra-low processing temperature, moderate CTE, low and high-frequency dielectric properties suggest that the presented Pb-free LNKM glass could be a good candidate for ULTCC applications as well as an encapsulated device fabrication with less environmental impact.

CONCLUSIONS

The present paper discusses the preparation, characterization and properties of a distinct combination of $10Li_2O$-$10Na_2O$-$20K_2O$-$60MoO_3$ (LNKM) glass for ULTCC applications. The LNKM glass was developed by conventional glass melting and quenching process. The glass has ultra-low temperature glass transition at 198 °C and melting temperature of 350 °C. The developed glass shows the coefficient of thermal expansion of 17 ppm/°C in the temperature range of 25-300 °C. X-ray diffraction and Raman spectroscopic studies indicate that the glass is partially crystallized. The chemical and elemental composition of the glass is confirmed by X-ray photoelectron spectroscopy. The bulk glass sample heat

treated at 300 ^{o}C has relative permittivity of 5.07 and dielectric loss tangent of 0.006 at 1 MHz. At 9.97 GHz, the relative permittivity and dielectric loss tangent are 4.85 and 0.0009, respectively. The temperature variation of relative permittivity is 307 (20-100 ^{o}C) and 291 (25-85 ^{o}C) ppm/^{o}C respectively at 1 MHz and 9.97 GHz. The ultra-low temperature processing, good dielectric and thermal properties make this glass a suitable candidate for next generation electronics with less environmental impact.

ASSOCIATED CONTENT

Supporting Information

- Optical and photographic images of LNKM glass.
- High resolution spectrum of C 1s peak originating from the hydrocarbon impurities present at the surface of LNKM glass.

AUTHOR INFORMATION

Corresponding Author

*Dr. Jobin Varghese, Email: jobin.var@gmail.com

ACKNOWLEDGEMENT

The authors are thankful to European Research Council project No: 24001893 for financial support. The authors also acknowledge Mr. Santtu Heinilehto (Application Engineer) for XPS and Mr. Pekka Moilanen for Raman spectroscopy measurements. Author Tuomo Siponkoski appreciatively acknowledge the Riitta ja Jorma J. Takanen, KAUTE, Tauno Tönning and Ulla Tuominen foundations as well as Infotech Oulu Doctoral Program for financial support.

ABBREVIATIONS

LTCC - Low Temperature Co-fired Ceramics; ULTCC - Ultra Low Temperature Co-fired Ceramics; LNKM - $10Li_2O$-$10Na_2O$-$20K_2O$-$60MoO_3$; RF-Radio frequency; CTE - Coefficient of Thermal Expansion; TG - Thermo Gravimetric; DSC - Differential Scanning Calorimetry; XPS - X-ray Photoelectron Spectroscopy; XRD - X-ray Diffraction; ICDD – International Centre for Diffraction Data

REFERENCES

1. Maeder, T. Review of Bi_2O_3 - Based Glasses for Electronics and Related Applications, *Int. Mater. Rev.* **2013**, *58*, 3–40.

2. Bengisu, M. Borate Glasses for Scientific and Industrial Applications: A Review, *J. Mater. Sci*. **2016**, *51,* 2199–2242, DOI 10.1007/s10853-015-9537-4.
3. Rahmane, M.; Lacovangelo, C. Materials for Advanced Sodium Metal Halide Batteries, Leadership Summit. *American Ceramic Society*, **2010**, Baltimore.
4. Reis, S. T.; Pascual, M. J.; Brow, R. K.; Ray, C. S.; Zhang, T. Crystallization and Processing of SOFC Sealing Glasses, *In Journal of Non-Crystalline Solids*, **2010**, *356*, 3009–3012.
5. Jantunen, H.; Rautioaho, R.; Uusimäki, A.; Leppävuori, S. Compositions of $MgTiO_3$–$CaTiO_3$ Ceramics with Two Borosilicate Glasses for LTCC Technology, *J. Eur. Ceram. Soc.* **2000**, *20*, 2331–2336.
6. Jurków, D.; Maeder, T.; Dąbrowski, A.; Zarnik, M. S.; Belavič, D.; Bartsch, H.; Müller, J. Overview on Low Temperature Co-fired Ceramic Sensors, *Sensors Actuators A Phys.* **2015**, *233*, 125–146.
7. Menad, N.; Guignot, S.; van Houwelingen, J. A. New Characterization Method of Electrical and Electronic Equipment Wastes (WEEE), *Waste Manag.* **2013**, *33*, 706–713.
8. Sebastian, M. T.; Ubic, R.; Jantunen, H. Low-Loss Dielectric Ceramic Materials and Their Properties, *Int. Mater. Rev.* **2015**, *60*, 392-412.
9. Induja, I. J.; Abhilash, P.; Arun, S.; Surendran, K. P.; Sebastian, M. T. LTCC Tapes Based on Al_2O_3-BBSZ Glass with Improved Thermal Conductivity, *Ceram. Int.* **2015**, 41, 13572-13581.
10. Manu, K.; Sebastian, M. T. Tape casting of low permittivity Wesselsite–Glass Composite for LTCC Based Microwave Applications, *Ceram. Inter.* **2016**, *42*, 1210–1216.
11. Dernovsek, O.; Eberstein, M.; Schiller, W. A.; Naeini, A.; Preu, G.; Wersing, W. LTCC Glass-Ceramic Composites for Microwave Application, *J. Eur. Ceram. Soc.*, **2001**, *21*, 1693–1697.
12. Imanaka, Y. Multilayered Low Temperature Cofired Ceramics (LTCC) Technology, **2005**, Springer.
13. Sebastian, M. T.; Jantunen, H. Low Loss Dielectric Materials for LTCC Applications: A Review, *Inter. Mater. Rev*. **2008**, *53*, 57–90.

14. Manu, K. M.; Anjana, P. S.; Sebastian, M. T. Low Permittivity $SrCuSi_4O_{10}$ – LMZBS Glass Composite for LTCC Applications, *Matt. Lett.* **2011**, *65*, 565-567.

15. Honkamo, J.; Jantunen, H.; Subodh, G.; Sebastian, M. T.; Mohanan, P. Tape Casting and Dielectric Properties of $Zn_2Te_3O_8$-Based Ceramics with an Ultra-Low Sintering Temperature, *Int. J. Appl. Ceram. Technol.* **2009**, *6,* 531–536.

16. Palukuru, V. K.; Peräntie, J.; Jäntti, J.; Jantunen, H. Tunable Microwave Phase Shifters Using LTCC Technology with Integrated BST Thick Films, *Int. J. Appl. Ceram. Technol.* **2012**, *9*, 11–17.

17. Varghese, J.; Gopinath, S.; Sebastian, M. T. Effect of Glass Fillers in $Cu_2ZnNb_2O_8$ Ceramics for Advanced Microwave Applications, *J. Mater. Chem. Phys.* **2013**, *137*, 811–815.

18. Sobocinski, M.; Leinonen, M.; Juuti, J.; Mantyniemi, N.; Jantunen, H. A Co-fired LTCC–PZT Monomorph Bridge Type Acceleration Sensor, *Sensors Actuators A Phys*. **2014**, *216*, 370–375.

19. Laurita, G., Page, K., Suzuki, S., Seshadri, R. Average and Local Structure of the Pb-Free Ferroelectric Perovskites (Sr, Sn) TiO_3 and (Ba, Ca, Sn) TiO_3, *Phys. Rev. B*, **2015**, *92*, 214109.

20. Varghese, J.; Joseph, T.; Sebastian, M. T.; Sol-gel Derived $TiSiO_4$ Ceramics for High-k Gate Dielectric Applications, *AIP Conference Proceedings*, **2011**, *1372*, 193-197.

21. Valant, M.; Suvorov, D.; Pullar, R. C.; Sarma, K.; Alford, N. M. A Mechanism for Low-Temperature Sintering, *J. Eur. Ceram. Soc.* **2006**, *26*, 2777–2783.

22. Kamba, S.; Noujni, D.; Pashkin, a.; Petzelt, J.; Pullar, R. C.; Axelsson, A.-K.; McN Alford, N. Low-Temperature Microwave and THz Dielectric Response in Novel Microwave Ceramics, *J. Eur. Ceram. Soc.* **2006**, *26*, 1845–1851.

23. Yu, H.; Liu, J.; Zhang, W.; Zhang, S. Ultra-Low Sintering Temperature Ceramics for LTCC Applications: A Review, *J. Mater. Sci. Mater. Electron.* **2015**, 1–10, doi: 10.1007/s10854-015-3282-y.

24. Abhilash, P.; Sebastian, M. T.; Surendran, K. P. Glass Free, Non-Aqueous LTCC Tapes of $Bi_4(SiO_4)_3$ with High Solid Loading, *J. Eur. Ceram. Soc.* (**2016**). doi:10.1016/j.jeurceramsoc.2016.02.019.

25. Thomas, D.; Abhilash, P.; Sebastian, M. T. Casting and Characterization of $LiMgPO_4$ Glass Free LTCC Tape for Microwave Applications, *J. Eur. Ceram. Soc.* **2013**, *33,* 87–93.

26. Sebastian, M. T.; Wang, H.; Jantunen, H. Low Temperature Co-fired Ceramics with Ultra Low Sintering Temperature: A Review, *Curr. Opin. Solid State Mater. Sci.,* In Press (**2016**), http://dx.doi.org/10.1016/j.cossms.2016.02.004.

27. Schott. Technical Glasses Physical and Chemical properties, 10.1016/B978-0-08-002597-1.50008-5.

28. Kähäri, H.; Teirikangas, M.; Juuti, J.; Jantunen, H. Dielectric Properties of Lithium Molybdate Ceramic Fabricated at Room Temperature, *J. Am. Ceram. Soc*. **2014**, *97*, 3378–3379.

29. Kähäri, H.; Teirikangas, M.; Juuti, J.; Jantunen, H. Improvements and Modifications to Room-Temperature Fabrication Method for Dielectric Li_2MoO_4 Ceramics*, J. Am. Ceram. Soc*. **2015**, *98*, 687–689.

30. Chen, M.-Y.; Juuti, J.; Hsi, C.-S.; Chia, C.-T.; Jantunen, H. Dielectric $BaTiO_3$–BBSZ Glass Ceramic Composition with Ultra-Low Sintering Temperature, *J. Eur. Ceram. Soc*. **2015**, *35*, 139–144.

31. Zhou, D.; Pang, L.-X.;, Qi, Z.-M.; Jin, B.-B.; Yao, X.; Novel Ultra-Low Temperature Co-Fired Microwave Dielectric Ceramic at 400 Degrees and its Chemical Compatibility with Base Metal, *Nature Sci. Rep.* **2014**, *4:5980*, doi: 10.1038/srep05980.

32. Zhou, D.; Randall, C. A.; Pang, L.-X.; Wang, H.; Wu, X.-G.; Guo, J.; Zhang, G.-Q.; Shui, L; Yao, X. Microwave Dielectric Properties of $Li_2(M^{2+})2Mo_3O_{12}$ and $Li_3(M^{3+})Mo_3O_{12}$ (M = Zn, Ca, Al, and In) Lyonsite-Related-Type Ceramics with Ultra-Low Sintering Temperatures, *J. Am. Cerm. Soc.* **2011**, *94*, 802–805.

33. Liao, Q.; Wang, Y.; Jiang, F.; Guo, D. Ultra-Low Fire Glass-Free $Li_3FeMo_3O_{12}$ Microwave Dielectric Ceramics, *J. Am. Cerm. Soc.* **2014**, *97*, 2394–2396.

34. Zhou, D.; Randall, C. A.; Wang, H.; Pang, L.-X.; Yao, X. Microwave Dielectric Ceramics in Li_2O–Bi_2O_3–MoO_3 System with Ultra-Low Sintering Temperatures, *J. Am. Ceram. Soc.* **2010**, *93*, 1096–1100.

35. Pang, L. -X.; Zhou, D.; Guo, J.; Yue, Z. –X.; Yao, X. Microwave Dielectric Properties of ($Li_{0.5}Ln_{0.5}$) MoO_4 (Ln= Nd, Er, Gd, Y, Yb, Sm, and Ce) Ceramics, *J. Am. Cerm. Soc.* **2015**, *98*, 130–135.

36. Zhou, D.; Li, W.-B.; Pang, L. -X.; Guo, J.; Qi, Z. -M.; Shao, T.; Yue, Z. -X.; Yao, X. Sintering Behavior and Dielectric Properties of Ultra-Low Temperature Fired Silver Molybdate Ceramics, *J. Am. Ceram. Soc.* **2014**, *97*, 3597–3601.

37. Wang, S. F.; Wang, T. R; Hsu, Y. F.; Lu, H. C.; Tsai, J. S. Ultra-Low-Fire $Te_2(Mo_{1-x}W_x)O_7$ Ceramics: Microstructure and Microwave Dielectric Properties, *J. Am. Cerm. Soc.* **2010**, *93*, 4071–4074.

38. Zhou, D.; Wang, H.; Pang, L. -X.; Randall, C. A.; Yao, X. Bi_2O_3–MoO_3 Binary System: An Alternative Ultralow Sintering Temperature Microwave Dielectric, *J. Am. Ceram. Soc.* **2009**, *92*, 2242–2246.

39. Xie, H.; Xi, H.; Li, F.; Chen, C.; Wang, X.; Zhou, D. Microwave Dielectric Properties of Pb_2MoO_5 Ceramic with Ultra-Low Sintering Temperature, *J. Eur. Ceram. Soc.* **2014**, *34*, 4089–4093.

40. Zhou, D.; Randall, C. A.; Pang, L. X. ; Wang, H.; Guo, J.; Zhang, G. Q. ; Wu, Y.; Guo, K. T.; Shui, L.; Yao, X. Microwave Dielectric Properties of $(ABi)_{1/2}$ MoO_4 (A= Li, Na, K, Rb, Ag) Type Ceramics with Ultra-Low Firing Temperatures, *Mater. Chem. Phys.* **2011**, *129*, 688–692.

41. Zhou, D.; Li, W. -B.; Guo, J.; Pang, L. -X.; Qi, Z. -M.; Shao, T.; Xie, H. -D.; Yue, Z. -X.; Yao, X. Structure, Phase Evolution, and Microwave Dielectric Properties of $(Ag_{0.5}Bi_{0.5})(Mo_{0.5}W_{0.5})O_4$ Ceramic with Ultralow Sintering Temperature, *Inorg. Chem.* **2014**, *53*, 5712–5716.

42. Lee, Y. C.; Chiu J. D.; Chen, Y. H. . Effects of Nb_2O_5 Doping on the Microwave Dielectric Properties and Microstructures of $Bi_2Mo_2O_9$ Ceramics, *J. Am. Cer. Soc.* **2013**, *96*, 1477–1482.

43. Chen, H.-R.; Lee, Y.-C.; Chen, G. H.; Chen, Y. H. Microwave Dielectric Properties and Microstructures of Y_2O_3-Doped $Bi_2Mo_2O_9$ Ceramics, *Ferroelectrics*, **2012**, *434*, 137–146.

44. Ihsan, M .; Wang, H.; Majid, S. R., Yang, J.; Kennedy, S. J.; Guo, Z.; Liu, H. K. MoO_2/Mo_2C/C Spheres as Anode Materials for Lithium Ion Batteries, *Carbon*, **2016**, *96*, 1200-1207.

45. Jia, X.; Jiang, Z.; Chen, X.; Zhou, J.; Pan, L.; Zhu, F.; Sun, Z.; Huang, S.Highly Efficient and Air Stable Inverted Polymer Solar Cells Using LiF Modified ITO Cathode and MoO_3/AgAl Alloy Anode, *ACS Appl. Mater. Interfaces*, **2016**, *8*, 3792-3799.

46. Varsamis, C. P. E.; Kamitsos, E. I.; Minami, T.; Machida, N. Investigation of CuI-Containing Molybdophosphate Glasses by Infrared Reflectance Spectroscopy, *J. Phys. Chem. C*, **2012**, *116*, 11671-11681.

47. Deb, B.; Ghosh, A. Silver Ion Dynamics in Ag_2S-Doped Silver Molybdate-Glass Nanocomposites: Correlation of Conductivity and Scaling with Structure, *J. Phy. Chem. C*, **2011**, *115*, 14141-14147.

48. Poirier, G.; Ottoboni, F. S. Redox Behavior of Molybdenum and Tungsten in Phosphate Glasses, *J. Phys. Chem. B*, **2008**, *112*, 4481-4487.

49. Karthikeyan, A.; Rao, K. J. Structure and Silver Ion Transport in AgI-Ag_2MoO_4 Glasses: A Molecular Dynamics Study, *J. Phys. Chem. B*, **1997**, *101*, 3105-3114.

50. John, E. C.; Wren, Greer, B. J.; Michaelis, V. K.; Higman C. S.; Kroeker, S. Multinuclear Magnetic Resonance Investigation of Crystalline Alkali Molybdates, *Inorg. Chem.* **2015**, *54*, 9853−9861.

51. Krupka, J; Gregory, A. P.; Rochard, O. C.; Clarke, R. N.; Riddle, B.; Baker-Jarvis, J. Uncertainty of Complex Permittivity Measurements by Split-Post Dielectric Resonator Technique, *J. Eur. Ceram. Soc.* **2001**, *10*, 2673–2676.

52. Chouard, N.; Caurant, D.; Maje´rus, O.; Dussossoy, J. L.; Klimin, S.; Pytalev, D.; Baddour-Hadjean, R.; Pereira-Ramos, J. P. Effect of MoO_3, Nd_2O_3, and RuO_2 on the Crystallization of Soda–Lime Aluminoborosilicate Glasses, *J. Mater. Sci.* **2015**, *50*, 219–241.

53. Miguel, A. M. M.; Maider, Z.; Elizabeth, C. M.; Aitor, E. B.; Teo´filo, R.; Montse, C. C. Composition and Evolution of the Solid-Electrolyte Interphase in $Na_2Ti_3O_7$ Electrodes for Na-Ion Batteries: XPS and Auger Parameter Analysis, *ACS Appl. Mater. Interfaces,* **2015**, *7*, 7801–7808.

54. Rastogi, R. S.; Vankar, V. D.; Chopra, K. L. Auger Electron Spectroscopy, X-ray Photoelectron Spectroscopy, and Electron Energy-Loss Spectroscopy Studies of $MoSi_2$, *J. Vac. Sci. Technol. A,* **1992**, *10*, 2822, http://dx.doi.org/10.1116/1.577917.

55. Nyholm, R.; Martensson, N. Core Level Binding Energies for the Elements Zr-Te (Z=40-52) *J. Phys. C Solid State Phys.* **1980**, *13*, L279.

56. Powell, C. J. Recommended Auger Parameters for 42 Elemental Solids *J. Electron Spectros. Relat. Phenomena,* **2012**, *185*, 1–3.

57. Sharma, D. D.; Rao, C. N. R. XPES Studies of Oxides of Second- and Third-Row Transition Metals Including Rare Earths, *J. Electron. Spectrosc. Relat. Phenom.* **1980**, *20*, 25-45.

58. Turner, N. H.; Single, A. M. Determination of Peak Positions and Areas from Wide-Scan XPS Spectra, *Surf. Interface Anal.* **1999**, *15*, 215-222.

59. Barr, T. L.; Fries, C. G.; Cariati, F.; Bart, J. C. J.; Giordano, N. A Spectroscopic Investigation of Cerium Molybdenum Oxides, *J. Chem. Soc., Dalt. Trans*. **1983**, 1825–1829, doi: 10.1039/DT9830001825.

60. Nesbitt, H. W.; Bancroft, G. M.; Henderson, G. S; Ho, R.; Dalby, K. N.; Huang, Y.; Yan, Z. Bridging, Non-Bridging and Free (O^{2-}) Oxygen in Na_2O-SiO_2 Glasses: An X-ray Photoelectron Spectroscopic (XPS) and Nuclear Magnetic Resonance (NMR) Study, *J. Non. Cryst. Solids,* **2011**, *357*, 170–180.

61. Nefedov, V. I.; Firsov, M. N.; Shaplygin, I. S. Electronic Structures of $MRhO_2$, MRh_2O_4, $RhMO_4$ and Rh_2MO_6 on the Basis of X-ray Spectroscopy and {ESCA} Data *J. Electron Spectros. Relat. Phenomena,* **1982**, *26*, 65–78.

62. Sawyer, R.; Nesbitt, H. W.; Secco. R. A. High Resolution X-ray Photoelectron Spectroscopy (XPS) Study of K_2O-SiO_2 Glasses: Evidence for Three Types of O and at Least Two Types of Si, *J. Non. Cryst. Solids,* **2012**, *358*, 290–302.

63. Brezesinski, T.; Wang, J.; Tolbert, S. H.; Dunn, B. Ordered Mesoporous α-MoO_3 with Iso-Oriented Nanocrystalline Walls for Thin-Film Pseudocapacitors, *Nat. Mater.* **2010**, *9*, 146–151.

64. Perry, A.; Spevack, S. M. Reactivity and Stability of Sulphided Thin Films of Molybdenum to Dry Air, *Appl. Catal.* **1990**, *64*, 191–207.

65. Seguin, L.; Figlarz, M.; Cavagnat, R.; Lassègues, J. –C.; Infrared and Raman spectra of MoO_3 Molybdenum Trioxides and $MoO_3 \cdot xH_2O$ Molybdenum Trioxide Hydrates, *Spectrochim. Acta Part A*, **1995**, *51*, 1323–1344.

66. Voronko, Y. K.; Sobol, A. A.; Shukshin. V. E. Raman Scattering Study of Molten Alkali-Metal Molybdates and Tungstates Rich in Basic Oxides, *Inorg. Mater.* **2014**, *15*, 837–843.

67. Du, X.; Dong, L.; Li, C.; Liang, Y.; Chen, Y. Diffuse Reflectance Infrared Fourier Transform and Raman Spectroscopic Studies of MoO_3 Dispersed on CeO_2 support, *Langmuir*, **1999**, *15*, 1693–1697.

68. Santagneli, S. H.; de Araujo, C. C.; Strojek, W.; Eckert, H.; Poirier, G.; Ribeiro, S. J. L.; Messaddeq, Y. Structural Studies of $NaPO_3$−MoO_3 Glasses by Solid-State Nuclear Magnetic Resonance and Raman Spectroscopy, *J. Phys. Chem. B,* **2007**, *111*, 10109–10117.

69. Wu, J. L.; Huang, H. L. Microwave Properties of Zinc, Barium, and Lead Borosilicate Glasses, *J. Non. Cryst. Solids,* **1999**, *260*, 116–124.

70. Hou, J.; Vaish, R.; Qu, Y.; Krsmanovic, D.; Varma, K. B. R.; Kumar, R. V. Dielectric Relaxation and Electrical Conductivity in Bi_5NbO_{10} Oxygen Ion Conductors Prepared by A Modified Sol–Gel Process, *J. Power Sources,* **2010**, *195*, 2613–2618.

71. Murawski, L.; Barczyński, R. J. Electronic and Ionic Relaxations in Oxide Glasses, *Solid State Ionics*, 2005, *176*, 2145–2151.

72. Muthupari, S.; Raghavan, S. L.; Rao, K. J. Electrical Transport Studies in Alkali Borovanadate Glasses, *J. Phys. Chem.* **1996**, *100*, 4243-4250.

Structural, Dielectric and Thermal Properties of Pb Free Molybdate Based Ultra-Low Temperature Glass

Jobin Varghese*, Tuomo Siponkoski, Merja Teirikangas, Mailadil Thomas Sebastian, Antti Uusimäki and Heli Jantunen

TOC Synopsis: Microwave dielectric properties of ultra-low temperature LNKM glass. It has low glass transition temperature of 198 °C, relative permittivity of 4.85, low dielectric loss of 0.0009 and low CTE 17 ppm/°C. The ultra-low temperature processing, good dielectric and thermal properties make this glass a suitable candidate for next generation electronics with less environmental impact.

TOC Graph